

# On the use of nonrigid-molecular symmetry in nuclear motion computations employing a discrete variable representation: A case study of the bending energy levels of $\text{CH}_5^+$

Csaba Fábri, Martin Quack, and Attila G. Császár

Citation: *The Journal of Chemical Physics* **147**, 134101 (2017); doi: 10.1063/1.4990297

View online: <http://dx.doi.org/10.1063/1.4990297>

View Table of Contents: <http://aip.scitation.org/toc/jcp/147/13>

Published by the [American Institute of Physics](#)

---

## Articles you may be interested in

[The aug-cc-pVnZ-F12 basis set family: Correlation consistent basis sets for explicitly correlated benchmark calculations on anions and noncovalent complexes](#)

*The Journal of Chemical Physics* **147**, 134106 (2017); 10.1063/1.4998332

[Connections between variation principles at the interface of wave-function and density-functional theories](#)

*The Journal of Chemical Physics* **147**, 134107 (2017); 10.1063/1.4985883

[A coherent discrete variable representation method on a sphere](#)

*The Journal of Chemical Physics* **147**, 094101 (2017); 10.1063/1.4996891

[A stimulated emission study of the ground state bending levels of  \$\text{BH}\_2\$  through the barrier to linearity and ab initio calculations of near-spectroscopic accuracy](#)

*The Journal of Chemical Physics* **147**, 124303 (2017); 10.1063/1.4990760

[Experimental and theoretical studies of the reactions of ground-state sulfur atoms with hydrogen and deuterium](#)

*The Journal of Chemical Physics* **147**, 134302 (2017); 10.1063/1.4991418

[Detection and structural characterization of nitrosamide  \$\text{H}\_2\text{NNO}\$ : A central intermediate in de \$\text{NO}\_x\$  processes](#)

*The Journal of Chemical Physics* **147**, 134301 (2017); 10.1063/1.4992097

---

**Scilight**

Sharp, quick summaries illuminating  
the latest physics research

Sign up for FREE!

AIP  
Publishing

# On the use of nonrigid-molecular symmetry in nuclear motion computations employing a discrete variable representation: A case study of the bending energy levels of $\text{CH}_5^+$

Csaba Fábri,<sup>1,2</sup> Martin Quack,<sup>2</sup> and Attila G. Császár<sup>1,3</sup>

<sup>1</sup>Laboratory of Molecular Structure and Dynamics, Institute of Chemistry, Eötvös University,

Pázmány Péter sétány 1/A, H-1117 Budapest, Hungary

<sup>2</sup>Physical Chemistry, ETH Zürich, CH-8093 Zürich, Switzerland

<sup>3</sup>MTA-ELTE Complex Chemical Systems Research Group, P.O. Box 32, H-1518 Budapest 112, Hungary

(Received 14 June 2017; accepted 2 September 2017; published online 2 October 2017)

A discrete-variable-representation-based symmetry adaptation algorithm is presented and implemented in the fourth-age quantum-chemical rotational-vibrational code GENIUSH. The utility of the symmetry-adapted version of GENIUSH is demonstrated by the computation of seven-dimensional bend-only vibrational and rovibrational eigenstates of the highly fluxionally symmetric  $\text{CH}_5^+$  molecular ion, a prototypical astructural system. While the numerical results obtained and the symmetry labels of the computed rovibrational states of  $\text{CH}_5^+$  are of considerable utility by themselves, it must also be noted that the present study confirms that the nearly unconstrained motion of the five hydrogen atoms orbiting around the central carbon atom results in highly complex rotational-vibrational quantum dynamics and renders the understanding of the high-resolution spectra of  $\text{CH}_5^+$  extremely challenging. *Published by AIP Publishing.* <https://doi.org/10.1063/1.4990297>

## I. INTRODUCTION

Symmetry plays a fundamental and very important role in all scientific disciplines<sup>1</sup> and even beyond science.<sup>2</sup> In the fields of theoretical molecular spectroscopy and quantum dynamics (QD), the following aspects motivate the detailed consideration of symmetry: (a) it is often indispensable to have knowledge about the symmetry properties and irreducible representation labels of rovibronic eigenstates as this information is necessary for nuclear spin statistical weight considerations, especially during the interpretation of high-resolution spectra; (b) appropriate consideration of symmetry renders rotational-vibrational QD computations more efficient by reducing the dimension of the basis and results in the automatic assignment of irreducible representation labels to the computed rovibronic eigenstates; (c) generation of Hamiltonian blocks corresponding to different irreducible representations reduces the density of energy eigenvalues and thus improves the convergence properties of the iterative Lanczos eigensolver,<sup>3</sup> often employed to compute the desired rovibronic eigenstates during variational-like solution of the time-independent Schrödinger equation (TISE); and (d) symmetries and approximate symmetries determine the (approximate) constants of motion and selection rules in kinetic radiative and nonradiative state-to-state transitions and reactions and define the time scales for the primary processes.<sup>1</sup>

Symmetry groups of the rotational-vibrational Hamiltonian encompass permutations of identical nuclei and the operation of space inversion, giving rise to the so-called complete nuclear permutation inversion (CNPI) and molecular symmetry (MS) groups.<sup>1,4–9</sup> While symmetry has been used<sup>10–14</sup> when solving the TISE in a discrete variable

representation (DVR)<sup>15,16</sup> or employing the symmetry-adapted Lanczos method<sup>17–23</sup> and also to systematically formulate full-dimensional molecular potential energy hypersurfaces,<sup>24,25</sup> to the best of the authors' knowledge, only two general symmetry-adapted nuclear motion codes have been developed until now.<sup>26,27</sup>

The highly nonrigid molecular ion  $\text{CH}_5^+$ , named methonium (see Fig. 1), is the prototype of pentacoordinated nonclassical carbonium ions which show a rich chemistry. Although  $\text{CH}_5^+$  was discovered in mass spectrometric studies more than 60 years ago,<sup>28</sup> the true fame of  $\text{CH}_5^+$  in chemistry is due to its role in acid-catalyzed transformations of hydrocarbons, a research area pioneered by Olah and his co-workers.<sup>29–36</sup> It turns out that more recently also the quantum theory (also highly nonclassical in a different sense) of the spectroscopy and energy levels of  $\text{CH}_5^+$  provides a rich and very challenging playground for new method developments. The focus of the present work is on the symmetry aspects of the QD of methonium.  $\text{CH}_5^+$  is particularly suitable as a testing ground for such investigations due to the great current interest in its high-resolution molecular spectroscopy and the availability of accurate computational results with which we can compare the rovibrational eigenstates and energy levels.<sup>37–39</sup>  $\text{CH}_5^+$  became not only famous but also infamous in circles of high-resolution molecular spectroscopists, owing to the highly unusual characteristics of the nuclear dynamics of  $\text{CH}_5^+$  associated with rovibrational excitation and the resulting complexity of its spectra even at very low temperatures (few K). This is due to the fact that  $\text{CH}_5^+$  is an important member of the class of astructural molecules, like dimethyl acetylene,<sup>40,41</sup>  $\text{H}_5^+$  and its deuterated isotopomers,<sup>42–44</sup> as well as  $\text{CH}_4 \cdot \text{H}_2\text{O}$  and its deuterated isotopomers.<sup>45,46</sup>

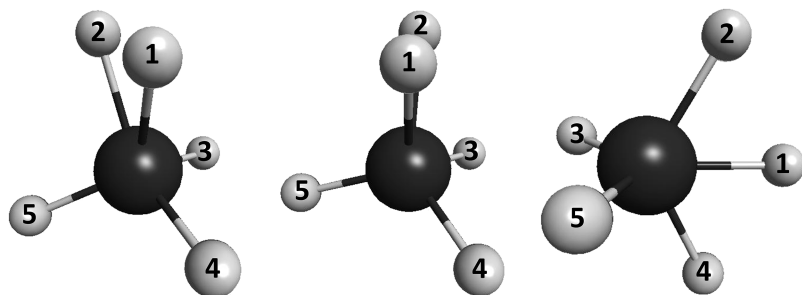


FIG. 1. Equilibrium (left) and two transition state structures (middle and right) of  $\text{CH}_5^+$ .

The structure and especially the high-resolution rovibrational spectra of  $\text{CH}_5^+$  have been investigated in considerable detail. It was even declared that variational nuclear-motion computations will not be able to help experimentalists to unravel the complex rovibrational spectra of  $\text{CH}_5^+$  for many decades.<sup>47</sup> The difficulties are related to the following: (a) it has been difficult to compute rovibrational spectra of molecules having six atoms; (b) the potential energy surface (PES) of  $\text{CH}_5^+$  is characterized by not one or a few but 120 equivalent minima; (c) the minima are separated by exceedingly small barriers, allowing facile exchange of the nuclei; and (d) the tacitly assumed model of QD simulations, separation of the vibrational and rotational degrees of freedom, does not hold for  $\text{CH}_5^+$ . Oka and co-workers<sup>48</sup> were the first to report a high-resolution infrared (IR) spectrum of  $\text{CH}_5^+$ . This highly congested spectrum contains about 900 lines in the narrow range of 2770–3150  $\text{cm}^{-1}$ . Further experimental studies redefining the state-of-the-art in this field were conducted by Asvany *et al.*,<sup>49,50</sup> leading to the recent determination of experimental combination differences (CD)<sup>51,52</sup> yielding a large number of the lower rovibrational energy levels of the system.  $\text{CH}_5^+$  has also been discussed as an intermediate complex in the reaction  $\text{CH}_4 + \text{H}^+ \rightarrow \text{CH}_5^+ \rightarrow \text{H}_2 + \text{CH}_3^+$ , with the possibility of scrambling of all protons in that long-lived complex and nevertheless striking detailed state-to-state symmetry selection rules.<sup>5</sup>

Electronic structure studies<sup>53,54</sup> have revealed that the 120 equivalent minima on the PES of  $\text{CH}_5^+$  have  $C_s$  point-group symmetry: a  $\text{H}_2$  moiety sits on top of a pyramidalized  $\text{CH}_3$  tripod (left panel in Fig. 1, where protons 1 and 2 belong to the  $\text{H}_2$  subunit) forming a formally three-center two-electron bond. The corresponding dissociation energy to give  $\text{CH}_3^+ + \text{H}_2$  is computed to be high, about 15 000  $hc \text{ cm}^{-1}$ .  $\text{CH}_5^+$  has several low-energy transition states (TSs), only marginally hindering certain internal motions of the atoms. One of these TS structures is associated with the internal rotation of the  $\text{H}_2$  moiety (middle panel in Fig. 1), while the other hinders the flip motion that exchanges protons between the  $\text{H}_2$  and  $\text{CH}_3$  subunits (right panel in Fig. 1). The barrier heights corresponding to the internal rotation and flip TS structures are about 30  $hc \text{ cm}^{-1}$  ( $C_s$  point-group symmetry) and 300  $hc \text{ cm}^{-1}$  ( $C_{2v}$  point-group symmetry), respectively.

The development of  $\text{CH}_5^+$  potential energy and electric dipole moment hypersurfaces<sup>55,56</sup> paved the way for detailed theoretical investigations of the complex internal dynamics of  $\text{CH}_5^+$ . Early studies by Bunker and co-workers<sup>57–61</sup> considered the internal rotation and flip motions mentioned and aimed at computing the energy levels and the spectrum of  $\text{CH}_5^+$ . Other

theoretical studies include investigations of the structure and spectrum of  $\text{CH}_5^+$ ,<sup>62,63</sup> full and reduced-dimensional computations of energy levels and wave functions,<sup>37–39</sup> application of the particle on a sphere (POS) model to  $\text{CH}_5^+$ ,<sup>64–70</sup> and a series of diffusion quantum Monte Carlo (DQMC) investigations.<sup>71–76</sup> Further theoretical studies found that separation of rotational and vibrational degrees of freedom is not possible for the astructural  $\text{CH}_5^+$  molecule<sup>39,77</sup> and made significant progress in the qualitative interpretation of the peculiar energy level pattern of  $\text{CH}_5^+$  by proposing a 5D rotor model.<sup>78,79</sup>

The main objective of this paper has been to show how to extend the fourth-age quantum-chemical general rotational-vibrational GENIUSH code,<sup>80–82</sup> where GENIUSH stands for general (GE) rovibrational code with numerical (N), internal-coordinate (I), user-specified (US) Hamiltonians (H), so that it can handle symmetry-adapted DVR basis functions when solving the rotational-vibrational Schrödinger equation. The utility of the symmetry-adapted GENIUSH code is shown by computing symmetry-labeled energy levels and eigenstates of  $\text{CH}_5^+$ .

## II. THEORY

After a brief review of the GENIUSH protocol, needed to understand the later symmetry arguments, those developments are summarized which facilitate the computation of symmetry-adapted rovibrational energy levels and eigenstates of molecules. Then, we provide a detailed description of the new symmetry adaptation features, making our investigation of the low-lying energy levels of  $\text{CH}_5^+$  feasible.

### A. Solution of the rotational-vibrational Schrödinger equation

The rotational-vibrational Hamiltonian of a molecule (with  $D$  vibrational degrees of freedom) expressed in general internal coordinates has the form

$$\hat{H} = \hat{T} + \hat{V} = \frac{1}{2} \sum_{k=1}^{D+3} \sum_{l=1}^{D+3} \tilde{g}^{-1/4} \hat{p}_k^\dagger G_{kl} \tilde{g}^{1/2} \hat{p}_l \tilde{g}^{-1/4} + \hat{V}, \quad (1)$$

where  $\mathbf{G}$  is the inverse of the rotational-vibrational metric tensor,  $\tilde{g} = \det(\mathbf{G}^{-1})$ ,  $\hat{p}_k$  is the momentum conjugate to coordinate  $q_k$ ,  $\hat{T}$  is the rovibrational kinetic energy operator, and  $\hat{V}$  is the potential energy surface. The precise definitions of the different quantities in  $\hat{T}$  and the technical details how the Hamiltonian of Eq. (1) can be implemented into an efficient

computer code have been described.<sup>81,82</sup> The solution of the time-independent Schrödinger equation,

$$\hat{H}\psi_i = E_i\psi_i, \quad (2)$$

results in rovibrational energy levels  $E_i$  and rovibrational wave functions  $\psi_i$ . In order to perform practical nuclear-motion computations while excluding electronic motion and nuclear spin, appropriate sets of vibrational coordinates and basis functions have to be chosen. The GENIUSH code constructs the general and exact rovibrational kinetic energy operator numerically; thus, in combination with a pointwise representation in a multidimensional DVR vibrational basis set, it offers the flexibility of defining arbitrary vibrational coordinates and body-fixed frames.

As a next step, we present an alternative way of computing energy levels and wave functions with nonzero rotational angular momentum (colloquially called  $J > 0$  computations, where  $J$  is the quantum number describing overall rotation). The vibrational subspace (VS) method used by the current version of GENIUSH was implemented earlier in the DEWE program package,<sup>83</sup> and similar ideas have been adopted by other research groups<sup>84–90</sup> as well. First, the rotational-vibrational Hamiltonian,

$$\hat{H} = \hat{T} + \hat{V} = \hat{T}_v + \hat{T}_r + \hat{T}_{rv} + \hat{V} = \hat{H}_v + \hat{T}_r + \hat{T}_{rv}, \quad (3)$$

is expressed as the sum of the vibrational Hamiltonian ( $\hat{H}_v$ ), the rotational kinetic energy ( $\hat{T}_r$ ), and the rotational-vibrational coupling term ( $\hat{T}_{rv}$ , often called the Coriolis term). The latter two operators are defined as

$$\hat{T}_r = \frac{1}{2} \sum_{\alpha=1}^3 G_{\alpha+D, \alpha+D} \hat{J}_\alpha^2 + \frac{1}{2} \sum_{\alpha=1}^3 \sum_{\beta=\alpha+1}^3 G_{\alpha+D, \beta+D} [\hat{J}_\alpha, \hat{J}_\beta]_+ \quad (4)$$

and

$$\hat{T}_{rv} = \frac{1}{2} \sum_{\alpha=1}^3 \sum_{k=1}^D (\hat{p}_k^\dagger G_{k, \alpha+D} + G_{k, \alpha+D} \hat{p}_k) \hat{J}_\alpha, \quad (5)$$

where  $\hat{J}_\alpha$  is the  $\alpha$ th component of the overall angular momentum expressed in the body-fixed frame and  $[\hat{J}_\alpha, \hat{J}_\beta]_+ = \hat{J}_\alpha \hat{J}_\beta + \hat{J}_\beta \hat{J}_\alpha$ . The vibrational wave functions  $\Phi_i$  (satisfying the vibrational Schrödinger equation  $\hat{H}_v \Phi_i = E_{v,i} \Phi_i$ ) can be used for the compact expansion of rovibrational wave functions as

$$\psi = \sum_{i=1}^n \sum_{j=1}^{2J+1} c_{ij} \Phi_i R_j, \quad (6)$$

where  $n$  vibrational wave functions  $\Phi_i$  are combined with  $2J + 1$   $R_j$  rotational basis functions. In order to set up the VS Hamiltonian matrix for a given  $J$  value, the matrix elements

$$\langle \Phi_i R_j | \hat{H} | \Phi_k R_l \rangle = E_{v,i} \delta_{ik} \delta_{jl} + \langle \Phi_i R_j | \hat{T}_r + \hat{T}_{rv} | \Phi_k R_l \rangle \quad (7)$$

have to be evaluated. Diagonalization of the VS Hamiltonian yields approximate but usually sufficiently accurate rovibrational energy levels and wave functions (tested for semirigid molecules in Ref. 83).

The VS method is closely related to the rigid rotor decomposition (RRD) procedure developed in our group<sup>91</sup> and used for assigning approximate vibrational and rotational quantum labels to variationally computed rotational-vibrational eigenstates. The  $c_{ij}$  coefficients from Eq. (6), obtained directly

from the VS computations, are equivalent to overlaps between the rotational-vibrational eigenstates and basis states  $\Phi_i R_j$  in Eq. (6). If the  $R_j$  functions are chosen as the rigid rotor eigenfunctions of the molecule under investigation, the  $c_{ij}$  quantities are equivalent to the RRD coefficients defined in Ref. 91, and according to the RRD procedure, quantum numbers of the dominant  $\Phi_i R_j$  basis state are assigned to the rotational-vibrational eigenstate.

GENIUSH allows the user to employ the Eckart body-fixed frame<sup>92</sup> for arbitrary vibrational coordinates with either fixed or flexible reference structures.<sup>93,94</sup> In the present version of GENIUSH, the quaternion-based Eckart transformation algorithm of Ref. 95 is implemented. Other approaches for the application of the Eckart frame have also been reported.<sup>85,96–101</sup> At this point it must be emphasized that for the  $\text{CH}_5^+$  test computations detailed below, the body-fixed frame was not chosen according to the rotational Eckart condition.

## B. Symmetry considerations

The starting point of our discussion of the implementation of molecular symmetry within a DVR-based time-independent nuclear-motion protocol is the definition of the molecular symmetry (MS) group<sup>1,4–9</sup>  $G = \{g_i | i = 1, \dots, |G|\}$ , where  $|G|$  denotes the order of  $G$ , the  $g_i$  symmetry operations commute with the molecular Hamiltonian ( $[g_i, \hat{H}] = 0$ ), and  $G$  contains all feasible permutation-inversion symmetry operations from the complete nuclear permutation inversion (CNPI) group. An important consequence of this commutation relation regarding the eigenvalues  $E_i$  and eigenfunctions  $\psi_i$  of  $\hat{H}$  is that the  $n$ -fold degenerate  $\psi_{ij}$  eigenfunctions ( $j = 1, \dots, n$ ) corresponding to the same  $E_i$  span an  $n$ -dimensional irreducible representation of  $G$ . According to the grand orthogonality theorem (GOT),<sup>102</sup> basis functions spanning the  $\Gamma_\alpha$  irreducible representation can be generated by the projector

$$P_{\alpha j} = \frac{d_\alpha}{|G|} \sum_{i=1}^{|G|} \overline{D_{jj}^\alpha(g_i)} g_i, \quad (8)$$

where  $j = 1, \dots, d_\alpha$  labels orthonormal basis functions  $\kappa_j^\alpha$  spanning irreducible representation  $\Gamma_\alpha$  of dimension  $d_\alpha$ ,  $\mathbf{D}^\alpha(g_i)$  is the matrix representation of  $g_i$  in the  $\kappa_j^\alpha$  basis, and  $\overline{D_{jj}^\alpha(g_i)}$  means the complex conjugate of  $D_{jj}^\alpha(g_i)$ . As  $P_{\alpha j}$  is expressed as a linear combination of the group elements,  $P_{\alpha j}$  commutes with  $\hat{H}$ . In practical computations, the matrix representations of certain symmetry operations may not commute with the Hamiltonian matrix due to numerical errors.<sup>18–20,23</sup>

In order to obtain symmetry-adapted linear combinations of vibrational basis functions,  $P_{\alpha j}$  must act on the direct-product DVR basis functions. In what follows, we require that each DVR function (or equivalently the grid point associated with the selected DVR function) is mapped onto another DVR function (or onto itself in special cases) by any of the  $g_i$  symmetry operations. This requirement implies that a smaller and nonunique set of DVR basis functions, termed the generator set, exists so that each DVR basis function can be generated by applying a symmetry operation on a member of the

generator set. Let us denote members of the generator set by  $\phi_i^{(a)}$ , where a given value of index  $a$  collects functions from the generator set having the same transformation properties (i.e., functions sharing the same index  $a$  are transformed by the symmetry operations in the same way). Other basis functions can be generated by applying symmetry operations on  $\phi_i^{(a)}$ , the functions  $g_j\phi_i^{(a)}$  with fixed  $i$  and  $a$  are called symmetry equivalent basis functions (they form equivalence classes in a mathematical sense).

Symmetry equivalent basis functions with fixed  $i$  and  $a$  form an invariant subspace with respect to the  $g_j$  symmetry operations in the linear space spanned by the vibrational basis functions,

$$g_k(g_j\phi_i^{(a)}) = (g_k g_j)\phi_i^{(a)} = g_l\phi_i^{(a)}, \quad (9)$$

where  $g_k g_j = g_l \in G$ . Matrices representing the symmetry operations  $g_k$  can be set up by noting that

$$\begin{aligned} \langle g_j\phi_i^{(a)} | g_k g_l \phi_i^{(a)} \rangle &= \langle \phi_i^{(a)} | g_j^{-1} g_k g_l \phi_i^{(a)} \rangle \\ &= \begin{cases} 1, & \text{if } g_j^{-1} g_k g_l \phi_i^{(a)} = \phi_i^{(a)} \\ 0, & \text{otherwise} \end{cases}, \quad (10) \end{aligned}$$

where we exploit that symmetry operations are unitary operators and vibrational basis functions are orthonormal. Although the dimension of symmetry operation matrices equals the dimension of the vibrational basis, they have a sparse block structure due to the low-dimensional invariant subspaces spanned by functions of the type  $g_j\phi_i^{(a)}$ . If no pair or larger group of symmetry operations maps  $\phi_i^{(a)}$  onto the same function, namely,

$$\exists g_j, g_k \in G : g_j\phi_i^{(a)} = g_k\phi_i^{(a)}, \quad (11)$$

then the dimension of the corresponding invariant subspace is equal to  $|G|$  and  $g_k\phi_i^{(a)}$  ( $k = 1, \dots, |G|$ ) span a  $|G|$ -dimensional representation  $\Gamma$  of  $G$ . The characters of this representation are

$$\chi^\Gamma(g_k) = \sum_{j=1}^{|G|} \langle g_j\phi_i^{(a)} | g_k g_j \phi_i^{(a)} \rangle = |G| \delta_{g_k, E}, \quad (12)$$

where  $E$  is the identity element of  $G$ . This equation can be used to decompose  $\Gamma$  into its constituent irreducible representations,

$$n_\alpha^\Gamma = \frac{1}{|G|} \sum_{k=1}^{|G|} \overline{\chi^\Gamma(g_k)} \chi^\alpha(g_k) = \frac{1}{|G|} |G| d_\alpha = d_\alpha. \quad (13)$$

When Eq. (11) does not hold, Eq. (13) is not valid. Note that further general group-theoretical considerations are presented in Appendix A.

The next step, after setting up the matrix representations of the symmetry operations  $g_i$  and the projectors  $P_{\alpha j}$ , is to construct symmetry-adapted vibrational basis functions. It turns out that in the case of abelian MS groups, it is sufficient to apply  $P_{\alpha j}$  on functions of the generator set ( $\phi_k^{(a)}$ ); this will automatically provide all orthogonal symmetry-adapted basis functions. However, if the MS group is not abelian, it becomes necessary to project not only  $\phi_k^{(a)}$  but also other  $g_i\phi_k^{(a)}$  symmetry-equivalent functions. As the projected functions are not necessarily linearly independent, the Gram–Schmidt algorithm is applied to obtain all orthonormal symmetry-adapted

basis functions (note that this is also true for our  $\text{CH}_5^+$  computations). We select one  $j$  value in  $P_{\alpha j}$  for degenerate irreducible representations, and in what follows, we drop  $j$  and  $a$  from  $P_{\alpha j}\phi_k^{(a)}$  in order to simplify our notation. Symmetry-adapted basis functions for the irreducible representation  $\Gamma_\alpha$  are defined as

$$\rho_i^\alpha = \sum_k A_{ik}^\alpha \phi_k, \quad (14)$$

where  $\mathbf{A}^\alpha$  is a sparse unitary matrix that defines symmetry-adapted basis functions and has a sparse block structure due to the low-dimensional invariant subspaces.

These considerations lead to the following matrix-vector multiplication algorithm needed by the Lanczos eigensolver:<sup>3</sup>

$$y_i^\alpha = \sum_j \langle \rho_i^\alpha | \hat{H} | \rho_j^\alpha \rangle x_j^\alpha = \sum_k A_{ik}^\alpha \sum_l \langle \phi_k | \hat{H} | \phi_l \rangle \sum_j A_{jl}^\alpha x_j^\alpha, \quad (15)$$

where summations are evaluated consecutively (a similar idea was employed in Ref. 103). First, an input vector  $\mathbf{x}^\alpha$  from irreducible representation  $\Gamma_\alpha$  is decompressed (sum over  $j$ , corresponds to a basis transformation to the original unsymmetrized vibrational basis), then the resulting full-dimensional vector is multiplied by the Hamiltonian matrix (in the unsymmetrized basis, sum over  $l$ ), and finally the full-dimensional result vector is compressed to yield the symmetry-adapted output vector  $\mathbf{y}^\alpha$  (sum over  $k$ , basis transformation from the unsymmetrized basis to the symmetry-adapted basis). Thus, while the dimension of the Lanczos vectors is reduced due to symmetry, the second step still involves a multiplication with the Hamiltonian represented in the unsymmetrized vibrational basis. Although it is possible to evaluate matrix-vector products directly in the symmetry-adapted basis, we have found that it is more convenient to apply the matrix-vector product algorithm outlined in Eq. (15). Representing the Hamiltonian in the symmetry-adapted basis would render both the kinetic and potential energy matrix elements more complicated as it is not trivial to deal with the resolutions of identity inserted between the momentum operators  $\hat{p}_k$  and the matrix elements  $G_{kl}$  (see Ref. 81 for further explanation), and the potential energy matrix does not necessarily assume a diagonal form in the symmetry-adapted basis.

The matrix-vector multiplication algorithm can be rendered more efficient by taking the sum of the  $\mathbf{v}^\alpha$  decompressed vectors (denoted by  $\mathbf{v}$ ) and carrying out the full-dimensional matrix-vector multiplication only once for  $\mathbf{v}$ . The scheme of the modified algorithm takes the form

$$\begin{aligned} v_l^\alpha &= \sum_j A_{jl}^\alpha x_j^\alpha, \\ \mathbf{w} &= \mathbf{H}\mathbf{v} = \sum_\alpha \mathbf{H}\mathbf{v}^\alpha, \\ y_i^\beta &= \sum_k A_{ik}^\beta w_k, \end{aligned} \quad (16)$$

where the number of  $\mathbf{H}\mathbf{v}$  matrix-vector products is obviously reduced by a factor of  $n$  compared to Eq. (15), if  $n$  irreducible representations are calculated at the same time. Although  $\mathbf{w}$  does not transform according to a single irreducible representation, multiplication of  $\mathbf{w}$  with  $\mathbf{A}^\beta$  in the third line of Eq. (16) projects out the component that transforms according to  $\Gamma_\beta$

(see Appendix B for the detailed proof). Note that the key idea behind Eq. (16) is the same as that of the symmetry-adapted Lanczos method.<sup>17–23</sup>

It is apparent that the symmetry-adapted version of GENIUSH provides degenerate energy levels only once since projectors [ $P_{\alpha j}$ , defined by Eq. (8)] are applied with a single  $j$  index. This implies that we get only one wave function ( $\psi_{ij}$ ) for each degenerate manifold of dimension  $d_{\alpha}$ . The missing  $d_{\alpha} - 1$  wave functions can be obtained by applying symmetry operations on  $\psi_{ij}$  and generating an orthonormal basis from the  $g_k \psi_{ij}$  functions, similar to Ref. 37.

It is important to emphasize that the algorithm presented is completely general. The only limitation is that the image of each direct-product grid point generated by any kind of symmetry operation has to be an element of the multidimensional DVR grid. This requirement is vital for the feasibility of the simple and efficient approach outlined above. Unfortunately, it often limits the practically applicable symmetry group to a subgroup of the full molecular symmetry group.

### III. TECHNICAL DETAILS ABOUT COMPUTATIONS ON CH<sub>5</sub><sup>+</sup>

In order to construct the kinetic energy operator, one has to specify a set of vibrational coordinates. Our computations on CH<sub>5</sub><sup>+</sup> employ the well-known orthogonal Radau polyspherical coordinates.<sup>104</sup> The five Radau vectors for a six-atom molecule can be parametrized with five distances ( $r_i$ ,  $i = 1, \dots, 5$ ), four polar angles ( $\theta_i$ ,  $i = 1, \dots, 4$ ), and three azimuthal angles ( $\varphi_i$ ,  $i = 1, \dots, 3$ ). The first and second Radau vectors are used to specify the body-fixed frame by attaching the body-fixed  $z$  axis to the first vector and defining the  $xz$  plane as the plane spanned by the first and the second vectors. In order to render the very challenging 12D(15D) vibrational(rovibrational) quantum dynamical problem tractable, we apply the  $r_i = 2.115\,96\,a_0$  constraint (this specific distance minimizes the potential under the constraint of equal Radau vector lengths<sup>37</sup>) and solve the resulting 7D bend problem variationally with the symmetry-adapted version of GENIUSH developed in Sec. II. The  $G_{kl}$  quantities in Eq. (1) require differentiation of the body-fixed position vectors  $\mathbf{x}_i$  with respect to the internal coordinates  $q_k$ .<sup>81</sup> The derivatives  $\mathbf{t}_{ik} = \partial \mathbf{x}_i / \partial q_k$  have been evaluated by GENIUSH analytically throughout this work. The five Radau vectors parametrized with the five fixed Radau distances and seven angular coordinates are differentiated with respect to the angles. Then, using the definition of the Radau coordinate system, the  $\mathbf{t}$  vectors of the C atom are obtained as linear combinations of the five  $\mathbf{t}$  vectors corresponding to the H atoms. Finally, the origin of the coordinate system is shifted to the center of mass (thus, the translational Eckart condition is fulfilled). The PES employed in this study was developed by Bowman and co-workers.<sup>55,56</sup> We used the modifications proposed in Sec. VII A of Ref. 37 to remove artifacts and imposed a potential ceiling of  $12\,000\,hc\,cm^{-1}$ , again in line with Ref. 37.

The 7D bend-only vibrational Schrödinger equation was solved using a direct-product DVR vibrational basis. In the case of  $\theta_i$ , a 1D minimum-energy path was generated by

optimizing all angles except the selected  $\theta_i$  coordinate. This 1D potential (shown in Appendix C) is needed to obtain potential-optimized<sup>105–107</sup> Legendre DVR points and basis functions for the  $\theta_i$  angles. Using the same 1D potential for all  $\theta_i$ s enforces that these coordinates are described by exactly the same grid points and DVR basis functions. This choice assures the feasibility of our symmetry-adapted approach. For the  $\varphi_i$  angles, we employed exponential DVR functions with equidistant grid points.<sup>108</sup> Although the boundary conditions are not satisfied in the direct-product DVR vibrational basis, it is well understood that DVR is able to provide accurate energy levels and wave functions for this type of problem.<sup>13,109</sup> The largest direct-product DVR basis used is built by 14 grid points for each  $\theta_i$  and 35 grid points for each  $\varphi_i$  coordinate; thus, the dimension of this vibrational basis equals  $14^4 \cdot 35^3 = 1\,647\,086\,000$ .

The full MS group of CH<sub>5</sub><sup>+</sup> is  $S_5^*$  (or  $G_{240}$ ), consisting of all  $5! = 120$  possible permutations of the five equivalent protons either with or without inversion. As permutations involving the first proton used to define the body-fixed  $z$  axis transform the internal coordinates in a much too complicated way, we omit these symmetry operations and retain only permutations of the other four protons ( $i = 2, \dots, 5$ ). This choice limits our treatment of symmetry to the  $S_4^*$  (or  $G_{48}$ ) MS group (see Ref. 5 for details and Appendix D of this paper for group-theoretical data). The idea of using  $S_4^*$  instead of  $S_5^*$  and the correlation rules between  $S_5^*$  and  $S_4^*$  appeared already in Ref. 37. Transformations of the internal coordinates under the symmetry operations of  $S_4^*$  can be derived in a straightforward manner by considering the general polyspherical coordinate transformation rules given in Table I. Choosing equidistant  $\varphi_i$  grid points is essential in light of the coordinate transformation rules provided in Table I.

As the group  $S_5^*$  is the direct-product group  $S_5 \otimes S^*$  (where  $S^* = \{E, E^*\}$ ), and the subgroup  $S_4^*$  is constructed similarly, it is convenient to use the notation for symmetry species of pure permutations in  $S_5$  and  $S_4$  and indicate parity as the symmetry species in  $S^*$  by the exponent: + for positive parity

TABLE I. Transformation properties of polyspherical coordinates under the transposition ( $ij$ ). Indices  $i, j$ , and  $k$  label H atoms starting from 1. Note that only H atoms with  $i > 1$  are transformed by the symmetry operations (see text). Only coordinates changed by the transposition ( $ij$ ) are given in the table; missing coordinates are left unaltered by ( $ij$ ). The inversion symmetry operation ( $E^*$ ) changes each  $\varphi_{i-2}$  to  $2\pi - \varphi_{i-2}$  ( $i > 2$ ); other coordinates are not affected by  $E^*$ . Each group element from the molecular symmetry group can be written as a product of transpositions and inversion.

Type	Original	Transformed
$r$	$(r_i, r_j)$	$(r_j, r_i)$
$\theta$	$(\theta_{i-1}, \theta_{j-1})$ (For $i > 1, j > 1$ )	$(\theta_{j-1}, \theta_{i-1})$
$\varphi$	$(\varphi_{i-2}, \varphi_{j-2})$ (For $i > 2, j > 2$ )	$(\varphi_{j-2}, \varphi_{i-2})$
$\varphi$	$\varphi_{j-2}$ $\varphi_{k-2}$ ( $k \neq j$ ) (For $i = 2, j > 2, k > 2$ )	$2\pi - \varphi_{j-2}$ $\varphi_{k-2} - \varphi_{j-2}$

TABLE II. List of low-lying 7D  $J = 0$  bend terms (in  $\text{cm}^{-1}$ , referenced to the respective zero point wavenumbers given in the first row) with  $S_5^*$  symmetry labels. Terms degenerate in  $S_5^*$  are obtained from two different irreducible representations (irreps) of the  $S_4^*$  symmetry group, only average values of these term pairs are given in the table, and splittings between the two terms from each pair can be found in parentheses (see text in Sec. IV A for further explanation and Table III in Appendix D for the sublevel structure). 7D and 12D results are taken from Refs. 38 and 39, respectively, and they are compared to our own 7D results [given in column 7D (own)]. Terms of  $A_2^\pm$ ,  $G_2^\pm$ , and  $H_2^\pm$  symmetries are allowed by the Pauli exclusion principle; thus, they are set in bold.

$\Gamma$	7D (own)	7D <sup>38</sup>	12D <sup>39</sup>	$\Gamma$	7D (own)	7D <sup>38</sup>	12D <sup>39</sup>
$A_1^+$	4016.4 (0.0)	4018.5	10956.4	$G_2^-$	<b>9.8 (0.3)</b>	<b>9.9</b>	<b>13.9</b>
$H_1^+$	20.3 (0.3)	20.4	31.4	$H_2^-$	<b>41.1 (0.5)</b>	<b>41.1</b>	<b>57.1</b>
$G_1^+$	49.3 (0.2)	49.4	41.6	$I^-$	58.2 (0.4)	58.4	54.4
$H_2^+$	<b>59.1 (0.6)</b>	<b>59.3</b>	<b>69.4</b>	$G_2^-$	<b>112.3 (0.1)</b>	<b>112.7</b>	<b>101.1</b>
$I^+$	111.4 (0.3)	112.0	108.4	$H_1^-$	113.4 (0.1)	113.7	121.1
$H_1^+$	121.3 (0.2)	122.0	132.6	$H_2^-$	<b>139.1 (0.2)</b>	<b>139.4</b>	<b>189.9</b>
$G_1^+$	154.2 (0.1)	154.5	209.0	$A_2^-$	<b>197.8 (0.0)</b>	<b>198.1</b>	<b>252.3</b>
$H_2^+$	<b>268.8 (0.2)</b>	<b>268.8</b>	<b>375.6</b>	$I^-$	264.5 (0.0)	264.6	213.1
$G_1^+$	329.1 (0.0)	329.5	389.1	$I^-$	354.9 (0.3)	356.5	346.9
$I^+$	360.1 (0.3)	361.5	351.4	$G_1^-$	383.4 (0.4)	384.2	404.3
$G_2^+$	<b>370.4 (1.0)</b>	<b>372.1</b>	<b>238.0</b>	$H_2^-$	<b>384.3 (0.0)</b>		<b>475.4</b>
$H_1^+$	412.7 (2.3)		242.0	$I^-$	431.2 (2.0)	434.5	
$G_2^+$	<b>468.9 (1.3)</b>			$H_1^-$	452.3 (0.5)		303.5
$H_1^+$	483.5 (0.1)			$G_2^-$	<b>479.5 (0.3)</b>		<b>400.4</b>
$H_2^+$	<b>510.1 (0.5)</b>						
$I^+$	540.6 (0.9)		471.4				

and  $-$  for negative parity, following Refs. 1, 5, and 110; see also Tables II–IV. We note that other conventions exist in the literature.<sup>6,8</sup> As the nuclei  $^{12}\text{C}$  and  $^1\text{H}$  have positive parity, the parity of the rovibrational wave functions is also the total parity, and for the  $^{13}\text{C}$  nucleus with negative parity, the total parity is reversed (note that the parity of the electronic ground state function is positive).

Taking into account  $S_4^*$  symmetry during the dynamical computations results in a significant reduction in the dimension of the vibrational basis, dimensions of the symmetry-adapted vectors are 34 763 946 ( $A_1^+$ ), 33 899 460 ( $A_2^+$ ), 68 659 878 ( $E^+$ ), 102 497 724 ( $F_1^+$ ), 103 361 958 ( $F_2^+$ ), 34 708 135 ( $A_1^-$ ), 33 891 914 ( $A_2^-$ ), 68 596 717 ( $E^-$ ), 102 546 822 ( $F_1^-$ ), and 103 363 281 ( $F_2^-$ ) instead of 1 647 086 000. These numbers show that for the 1D, 2D, and 3D irreducible representations, the dimensions of the symmetry-adapted vectors are only about 2%, 4%, and 6% of the dimension of the unsymmetrized basis. This enormous reduction is crucial for our in-house Lanczos eigensolver as Lanczos vectors are stored in memory and orthogonalized over the course of the Lanczos iteration. For each irreducible representation of the  $S_4^*$  group, ten vibrational states and wave functions (counting degenerate states once) were computed and the resulting 200 vibrational eigenstates were then used for the VS expansion of rotational-vibrational eigenstates for low overall angular momentum quantum number values  $J = 1, 2, \text{ and } 3$ . The VS computations employed the body-fixed frame defined in the first paragraph of this section. The vibrational ( $J = 0$ ) and the VS ( $J > 0$ ) computations required about 600 gigabytes of memory and took about six weeks in total on a computer with 60 cores.

## IV. QUALITATIVE UNDERSTANDING OF THE ENERGY LEVEL PATTERN OF $\text{CH}_5^+$

In this section, we present 7D bend-only vibrational ( $J = 0$ ) and rotational-vibrational ( $J > 0$ ) results for the  $\text{CH}_5^+$  molecule and compare our energy levels to those available in the literature.<sup>37–39</sup> Besides numerical results, qualitative arguments regarding the energy level pattern of  $\text{CH}_5^+$  and the separability of rotations and vibrations are also discussed.

### A. 7D bend vibrational results

The low-lying 7D bend vibrational energy levels of  $\text{CH}_5^+$  computed as part of this study with the symmetry-adapted version of GENIUSH are given in Table II. As already mentioned in Sec. III, our treatment of symmetry is limited to the  $S_4^*$  symmetry group; therefore, it directly provides only  $S_4^*$  symmetry labels. Nevertheless,  $S_5^*$  symmetry labels can be generated without any ambiguity from  $S_4^*$  symmetry labels using the correlation rules given in Table III (Appendix D). These correlation rules reveal that each level degenerate in  $S_5^*$  is in fact obtained from two different irreducible representations of  $S_4^*$ . As we do not use the full symmetry group, energy levels that should be degenerate show small splittings. In Table II average values of the split energy levels are provided. Splittings are given there in parentheses and they can be used to assess the numerical accuracy of our results. The full set of energy levels labeled with  $S_4^*$  symmetry labels, obtained directly from the GENIUSH computations, is presented in Table VI (Appendix E). Comparing our energy levels [marked as 7D (own) in Table II] to the 7D results of Refs. 37 and 38 shows good agreement between the two sets of results and verifies the correctness of our approach and coding. Note that this comparison of reduced-dimensional results is sensible as we have adapted the vibrational coordinates and the “cut” bend potential described in Ref. 37. Although only eigenstates transforming according to irreducible representations  $A_2^\pm$ ,  $G_2^\pm$ , and  $H_2^\pm$  have nonzero spin-statistical weights, we give energy levels for all irreducible representations in Table II.

A first attempt to understand the highly peculiar vibrational energy level pattern of  $\text{CH}_5^+$  may consider tunneling among the 120 equivalent wells of the PES. In the limit of infinite barriers, one would expect 120-fold degeneracies in the energy spectrum. In the case of finite barriers, states localized in the 120 equivalent wells of the PES are allowed to interact and energy level splittings arise. Couplings due to tunneling can be taken into account in an approximate manner by an effective 120-dimensional tunneling matrix, whose rows and columns correspond to degenerate states localized in one of the 120 equivalent PES wells. Note that this approach usually neglects Hamiltonian matrix elements between localized basis states with different energies. More information on the tunneling matrix formalism can be found in Appendix A.

If couplings due to interactions between different PES wells are considered for the vibrational ground state manifold of  $\text{CH}_5^+$ , the 120 localized ground states mix and the 120-fold degeneracy is lifted partially, giving rise to the following energy level pattern (where the order of the irreducible representations does not reflect the energy order of the

eigenstates):  $A_1^+ \oplus A_2^- \oplus 3G_1^+ \oplus G_1^- \oplus G_2^+ \oplus 3G_2^- \oplus 3H_1^+ \oplus 2H_1^- \oplus 2H_2^+ \oplus 3H_2^- \oplus 3I^+ \oplus 3I^-$ . Within this model, one may assume that the lowest 120 vibrational energy levels form an isolated cluster and their symmetry labels reproduce the result of the symmetry analysis. Note that similar considerations were made by Kolbuszewski and Bunker,<sup>58</sup> who examined the effect of internal rotation and flip motions and combined the internal rotation and flip tunneling by using a matrix model. Their approximate treatment yielded 120 energy levels coming in four larger groups of 20, 40, 40, and 20 closely spaced levels, where each of these four groups corresponds to an internal rotation level split into either 20 or 40 sublevels by the flip tunneling. However, the energy level set computed by us does not exhibit the 120-member energy level groups suggested by the tunneling matrix formalism. While most of the lowest bend energy levels seem to belong to the hypothetical ground-state energy level cluster, at higher energies these states are intermingled with intruder states (identified by a simple symmetry argument). Thus, the tunneling matrix formalism fails to provide a sensible model for the interpretation of the energy level structure and a satisfactory description even of the ground-state vibrations of  $\text{CH}_5^+$ , most likely due to the low barriers separating the different wells of the PES. Finally, we note that two well-separated 30-member vibrational energy level clusters, ranging from 0.0  $\text{cm}^{-1}$  to 59.1  $\text{cm}^{-1}$  and from 112.3  $\text{cm}^{-1}$  to 197.8  $\text{cm}^{-1}$ , can be observed in Table II. The existence of these clusters will play an important role in examining rotational-vibrational energy level clustering in Sec. IV B.

One is tempted to resort to another simple model and think of  $\text{CH}_5^+$  as five uncoupled rotors perturbed by the PES. This zeroth-order model can be described by the simple Hamiltonian

$$\hat{H}_0 = B \sum_{i=1}^5 \hat{j}_i^2, \quad (17)$$

where  $B$  is the rotational constant of a single rotor ( $B = 13.36 \text{ cm}^{-1}$  from Ref. 37) and  $\hat{j}_i$  represents the angular momentum vector of the  $i$ th light proton orbiting on the surface of a sphere around the heavy C atom. The eigenproblem of  $\hat{H}_0$  can be solved analytically and yields

$$E_{j_1 m_1, j_2 m_2, j_3 m_3, j_4 m_4, j_5 m_5} = B \hbar^2 \sum_{i=1}^5 j_i(j_i + 1) \quad (18)$$

and

$$|j_1 m_1, j_2 m_2, j_3 m_3, j_4 m_4, j_5 m_5\rangle = \prod_{i=1}^5 |j_i m_i\rangle, \quad (19)$$

the zeroth-order eigenvalues and eigenvectors (labeled with angular momentum quantum numbers of the five uncoupled rotors), respectively. Despite the low barriers and the facile exchange between distinct equivalent minima, the motion of the protons is strongly correlated in a sense that any pair of protons approaching each other causes large potential energy values and vanishing wave function amplitudes at these geometries. This effect cannot be captured by the zeroth-order eigenfunctions of Eq. (19) based on spherical harmonics. The uncoupled rotor model provides the starting point for the particle on a sphere (POS) model.<sup>64–70</sup>

A promising and simple zeroth-order model has been published recently by Schmiedt *et al.*<sup>78,79</sup> to interpret the unusual energy level patterns of extremely flexible systems. They introduce the concept of super angular momentum and 5D rotations to molecular spectroscopy, combine two essentially unhindered large-amplitude internal rotations with overall rotations in the case of  $\text{CH}_5^+$ , and propose a simple Hamiltonian which contains only one parameter and is invariant under the symmetry operations of the  $\text{SO}(5)$  symmetry group. The 5D rotor model provides an interesting qualitative picture and is able to guide the assignment of experimental combination differences.<sup>52,78,79</sup>

## B. 7D bend rotational-vibrational results

In this subsection, we present our 7D rotational-vibrational results obtained with the VS procedure (200 vibrational basis states are employed, degenerate eigenstates are counted multiple times everywhere in this section, and Table VI contains the complete list of vibrational eigenstates included in the VS basis). As our  $J > 0$  energy levels are not fully converged, only a pictorial representation of the energy level pattern (not considering nuclear spin statistics) is shown in Fig. 2, the full list of the  $J > 0$  energy levels is provided in the [supplementary material](#). We stress that only qualitative conclusions can be drawn from the rotational-vibrational results published in this paper and our theoretical energy level differences should not be compared directly to their experimental counterparts published by Asvany *et al.*<sup>51,52</sup>

Figure 2 reveals unusual energy level patterns for all  $J$  values studied. It is obvious that the well-known rigid rotor energy level structure is inconsistent with the results displayed in Fig. 2 as rotational-vibrational energy levels do not seem to be stacked around vibrational energy level values. However, two well-separated energy level clusters for  $J = 1$  and 2 can be observed, in line with other studies.<sup>38,39</sup> It is striking to realize that  $30 \cdot (2J + 1)$  energy levels form each of these clusters. This observation suggests that although rotational-vibrational energy levels are not associated with a single vibrational eigenstate, levels from the first and second clusters can be assigned either to the first or to the second

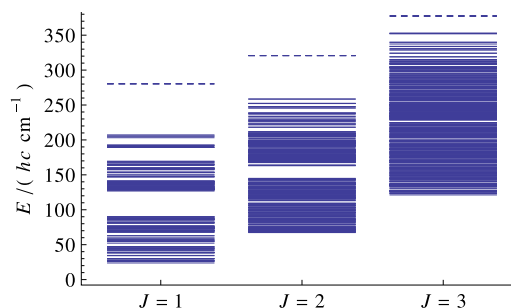


FIG. 2. Rotational-vibrational energy level patterns for  $J = 1, 2, 3$ . Each blue line represents an energy level; the two lowest energy level clusters of size  $30 \cdot (2J + 1)$  do not overlap for  $J = 1$  and  $J = 2$  (see Sec. IV B for further discussion). The dashed lines denote energy levels directly above the clusters of the lowest  $60 \cdot (2J + 1)$  energy levels.

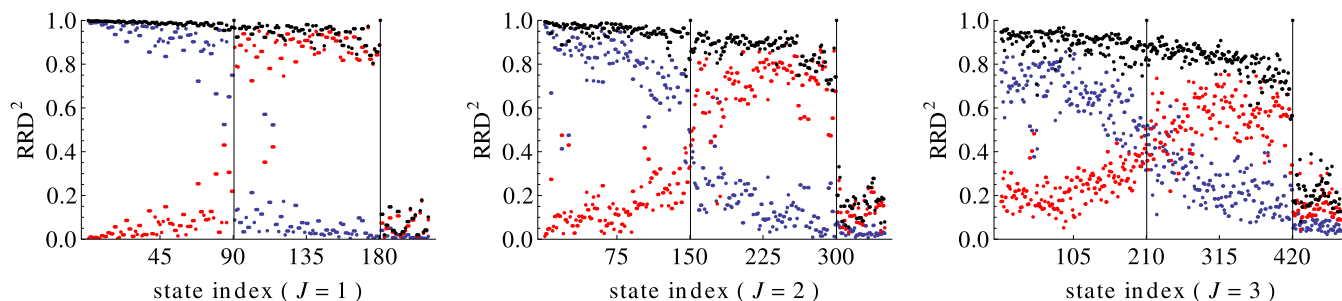


FIG. 3. Sums of RRD coefficient squares for rotational-vibrational eigenstates ( $J = 1, 2, 3$ ). The blue, red, and black marks represent sums of RRD coefficient squares associated with the first 30 [ $\text{RRD}(1,30)^2$ ], second 30 [ $\text{RRD}(31,60)^2$ ], and first 60 [ $\text{RRD}(1,60)^2$ ] vibrational eigenstates (see Sec. IV B for further explanation). The vertical black lines separate the first two energy level clusters of size  $30 \cdot (2J + 1)$ .

30-member vibrational energy level cluster, at least for the lowest  $J$  values.

To label the rovibrational energy levels, we carried out an RRD<sup>91</sup> analysis, mentioned briefly in Sec. II A. The RRD analysis clearly shows that the  $J > 0$  eigenstates are linear combinations of numerous  $\Phi_i R_j$  basis states [see Eq. (6)], meaning that rovibrational eigenstates cannot be assigned to a single vibrational eigenstate. A more thorough interpretation of the RRD results needs the sum of RRD coefficient squares defined as

$$\text{RRD}(n_1, n_2)^2 = \sum_{i=n_1}^{n_2} \sum_{j=1}^{2J+1} |c_{ij}|^2, \quad (20)$$

where the coefficients  $c_{ij}$  are components of the VS eigenvectors for a fixed  $J$  value and the sum is evaluated for vibrational eigenstates with  $i = n_1, \dots, n_2$ . Figure 3 shows the quantities  $\text{RRD}(1,30)^2$  (marked in blue),  $\text{RRD}(31,60)^2$  (marked in red), and  $\text{RRD}(1,60)^2$  (marked in black) for the first  $70 \cdot (2J + 1)$  rotational-vibrational eigenstates. Most of the first  $30 \cdot (2J + 1)$  rovibrational levels produce  $\text{RRD}(1,30)^2$  values close to 1.0, implying that the first rotational-vibrational energy level cluster can be assigned to the first 30-member group of vibrational eigenstates to a good approximation for  $J = 1$  and 2. Similarly, examining values of  $\text{RRD}(31,60)^2$  reveals that most energy levels from the second rovibrational cluster of size  $30 \cdot (2J + 1)$  can be assigned to the second 30-member vibrational energy level cluster. The widths of and gaps between the two rovibrational clusters for  $J = 1$  and 2 are in reasonable agreement with their counterparts published in Ref. 38, given in parentheses:  $(E_{90} - E_1)/(hc) = 66.2 \text{ cm}^{-1}$  ( $64.2 \text{ cm}^{-1}$ ),  $(E_{180} - E_{91})/(hc) = 80.1 \text{ cm}^{-1}$  ( $74.7 \text{ cm}^{-1}$ ), and  $(E_{91} - E_{90})/(hc) = 37.1 \text{ cm}^{-1}$  ( $39.5 \text{ cm}^{-1}$ ) for  $J = 1$ , and  $(E_{150} - E_1)/(hc) = 77.6 \text{ cm}^{-1}$  ( $69.4 \text{ cm}^{-1}$ ),  $(E_{300} - E_{151})/(hc) = 101.1 \text{ cm}^{-1}$  ( $75.5 \text{ cm}^{-1}$ ), and  $(E_{151} - E_{150})/(hc) = 18.2 \text{ cm}^{-1}$  ( $27.6 \text{ cm}^{-1}$ ) for  $J = 2$ .

It is also apparent from Fig. 3 that this simple picture based on separated energy level clusters breaks down as  $J$  increases. This is consistent with Fig. 2 as the first and second 210-member clusters for  $J = 3$  overlap and a significant fraction of the  $J = 3$   $\text{RRD}(1,30)^2$  and  $\text{RRD}(31,60)^2$  values are relatively far from 1.0 or 0.0, indicating stronger mixing. Note that these findings verify the group-theoretical result of Refs. 39 and 77 stating that separation of rotations and vibrations is not

possible due to fundamental reasons and rovibrational eigenstates can be characterized as superpositions of products of vibrational and purely rotational wave functions.

## V. DISCUSSION AND CONCLUSIONS

We developed a general DVR-based symmetry adaptation method and implemented it in the fourth-age quantum-chemical rotational-vibrational GENIUSH code. An important requirement of our approach is that each grid point must be mapped onto another grid point (or onto itself) by the symmetry operations of the molecular symmetry group. Therefore, for each new molecule, the rules describing the transformation of coordinates under different symmetry operations have to be derived and implemented by the user. Even though in many cases it is not possible to devise coordinates and DVR grids that allow the exploitation of the full MS group, an appropriately chosen subgroup of the full MS group can still be extremely helpful in reducing the computational cost and providing symmetry labels for the computed energy levels and eigenstates.

The symmetry-adapted version of GENIUSH has been employed to obtain rovibrational eigenstates for the  $\text{CH}_5^+$  molecular ion. The reasons for the choice of this example are at least threefold: (a)  $\text{CH}_5^+$  is a prototypical astructural system with complex internal dynamics; due to the low barriers to the internal rotation and flip motions, complete scrambling of the five protons is possible and all 120 equivalent minima on the PES are accessible; (b) the MS group of  $\text{CH}_5^+$  is the  $S_5^*$  (or  $G_{240}$ ) symmetry group containing all possible permutations of the five protons either with or without space inversion, making  $\text{CH}_5^+$  an ideal test case for a general symmetry-adaptation method; (c) interpretation of the experimental high-resolution spectra of  $\text{CH}_5^+$  is extremely challenging and conventional models used in molecular spectroscopy fail to provide an adequate zeroth-order description of the energy level structure of  $\text{CH}_5^+$ . We anticipate that the symmetry-adapted GENIUSH code will find other challenging applications, especially in the field of weakly-bound van der Waals complexes, in the near future.

Our vibrational and rotational-vibrational results utilizing a 7D bend-only model of  $\text{CH}_5^+$ , in accordance with other studies, confirm that the rovibrational energy level pattern of the  $\text{CH}_5^+$  molecule is highly peculiar, the approximate

separation of rotational and vibrational degrees of freedom is not possible, and the resulting transitions cannot be interpreted using the conventional techniques of molecular spectroscopy. Based on the numerical results and the tunneling matrix analysis described in this paper, we conclude that a simple tunneling analysis is not sufficient to explain the complex internal dynamics of  $\text{CH}_3^+$ . Our results for energy levels with  $J = 0$  agree well with the results of Ref. 38 and agree less well with those of Ref. 39. We confirm that the recently published 5D rotor model<sup>78,79</sup> combining two essentially free internal rotations with the overall rotations provides a correct qualitative description and it has been fruitful in the assignment of experimental combination differences.

## SUPPLEMENTARY MATERIAL

See [supplementary material](#) for the complete list of rotational-vibrational energy levels used for preparing Fig. 2.

## ACKNOWLEDGMENTS

This paper is dedicated to the memory of George A. Olah (Oláh György). The authors gratefully acknowledge discussions with Professor Joel Bowman and Professor Tucker Carrington and thank them for providing the potential energy and electric dipole moment hypersurfaces of  $\text{CH}_3^+$ . We are indebted to Dr. Viktor Szalay, Dr. Gábor Czakó, Dr. Edit Mátyus, Dr. Tamás Szidarovszky, Dr. János Sarka, and Dr. Oskar Asvany for useful discussions. We acknowledge the detailed comments by the reviewers, which helped clarify several aspects in the final manuscript. C.F. is grateful to COST Project No. CM1405, MOLIM: Molecules in Motion for funding a short-term scientific mission at Eötvös University in 2016. The work presented received support from NKFIH (Grant No. K119658).

## APPENDIX A: NUMBER OF EQUIVALENT MINIMA AND THE STRUCTURE OF THE TUNNELING MATRIX BASED ON GROUP THEORETICAL CONSIDERATIONS

In what follows, we outline a general group theoretical method to derive the number of distinct equivalent configurations and the structure of the effective Hamiltonian (or as it is usually called the tunneling matrix) describing the effect of tunneling between different potential wells. Note that the roots of this analysis go back a long time.<sup>111,112</sup>

Let  $G$  be the molecular symmetry group,  $H$  be a subgroup of  $G$ , and  $H < G$ .  $H$  is the symmetry group of a selected reference equilibrium structure (in other words, the equilibrium structure is invariant under the elements of  $H$ ). Following the formalism of elementary group theory, we define the left coset<sup>102</sup> of  $H$  in  $G$  with respect to  $g \in G$  as

$$gH = \{gh|h \in H\}. \quad (\text{A1})$$

Note that according to Lagrange's theorem, the order of  $H$  divides the order of  $G$ .

Here we restrict our treatment to the ground state and note that lifting this restriction poses no difficulties. Let  $\phi$  be a ground-state wave function localized in one of the equivalent

potential wells. Symmetry-equivalent functions localized in other wells can be obtained by letting symmetry operations  $g_i \in G$  act on  $\phi$ . Each symmetry operation can be decomposed as  $g_i = g_a h_j$ , where  $g_a$  generates the coset  $g_a H$ . As  $\phi$  transforms according to the totally symmetric irreducible representation of  $H$ ,

$$g_i \phi = g_a h_j \phi = g_a \phi. \quad (\text{A2})$$

Therefore, the number of linearly independent  $g_i \phi$  functions is equal to the number of cosets or equivalently  $|G|/|H|$ . The dimension of the ground state tunneling matrix is determined by  $|G|/|H|$ . As a consequence, there are  $|G|/|H|$  distinct equilibrium configurations, each of them is associated with a given coset and a set of rigid molecular states localized in a single potential well.

The structure and unique elements of the tunneling matrix can be obtained by employing the following rules:

$$\langle \phi | \hat{H} | g_a \phi \rangle = \langle (g_k^{-1} g_k) \phi | \hat{H} | g_a \phi \rangle = \langle g_k \phi | \hat{H} | g_k g_a \phi \rangle \quad (\text{A3})$$

and

$$\langle g_b \phi | \hat{H} | g_a \phi \rangle = \langle \phi | \hat{H} | g_b^{-1} g_a \phi \rangle, \quad (\text{A4})$$

with  $g_a, g_b, g_k \in G$  and taking into account that the tunneling matrix is symmetric. It is worth pointing out that Eq. (A4) means that the rows of the tunneling matrix are permutations of the first row corresponding to  $\phi$ .

Characters in the  $|G|/|H|$ -dimensional representation spanned by the functions  $g_a \phi$  can be expressed as

$$\chi(g_k) = \sum_{a=1}^{|G|/|H|} \langle g_a \phi | g_k g_a \phi \rangle = \sum_{a=1}^{|G|/|H|} \langle \phi | g_a^{-1} g_k g_a \phi \rangle, \quad (\text{A5})$$

where

$$\langle \phi | g_a^{-1} g_k g_a \phi \rangle = \begin{cases} 1, & \text{if } g_a^{-1} g_k g_a \in H \\ 0, & \text{otherwise} \end{cases}. \quad (\text{A6})$$

This representation is usually reducible. Standard group theoretical methods can be applied to construct symmetry-adapted functions and generate different symmetry blocks of the tunneling matrix. Diagonalization of these matrix blocks expressed in terms of unique matrix elements provides energy level patterns with symmetry labels and the associated eigenvectors approximating eigenstates of the system under investigation.

## APPENDIX B: PROOF OF THE VALIDITY OF THE MULTIPLICATION ALGORITHM OF EQ. (16)

Writing out summations for matrix-vector products in Eq. (16) yields

$$y_i^\beta = \sum_{jkl} A_{ik}^\beta H_{kl} \sum_{\alpha} A_{jl}^\alpha x_j^\alpha = \sum_{\alpha} \sum_j (\mathbf{A}^\beta \mathbf{H} (\mathbf{A}^\alpha)^T)_{ij} x_j^\alpha, \quad (\text{B1})$$

where summation over  $\alpha$  represents the summation of input vectors of different irreducible representations. According to Sec. II B, rows of the  $\mathbf{A}^\beta$  matrix (for irreducible representation  $\Gamma_\beta$ ) are linear combinations of rows of the projector matrix  $\mathbf{P}^\beta$  as orthonormal basis functions are generated

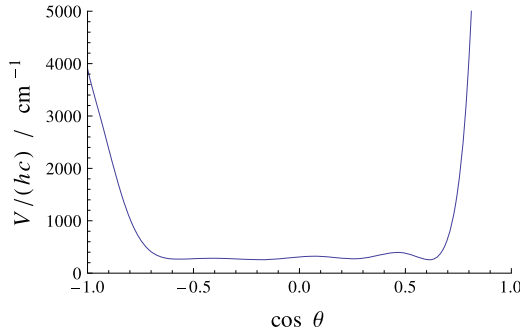


FIG. 4. 1D minimum energy path potential along one of the equivalent  $\theta_i$  coordinates (cosine of the angle is shown in the figure).

from the projected basis functions by the Gram–Schmidt algorithm,

$$A_{ik}^\beta = \sum_j c_{ij}^\beta P_{jk}^\beta. \quad (\text{B2})$$

It is straightforward to prove that the matrix  $\mathbf{A}^\beta \mathbf{H} (\mathbf{A}^\alpha)^\text{T}$  is proportional to  $\delta_{\alpha\beta}$ ,

$$\begin{aligned} (\mathbf{A}^\beta \mathbf{H} (\mathbf{A}^\alpha)^\text{T})_{ij} &= \sum_{mn} c_{im}^\beta c_{jn}^\alpha (\mathbf{P}^\beta \mathbf{H} \mathbf{P}^\alpha)_{mn} \\ &= \delta_{\alpha\beta} (\mathbf{A}^\alpha \mathbf{H} (\mathbf{A}^\alpha)^\text{T})_{ij}, \end{aligned} \quad (\text{B3})$$

where we exploit the relationships  $\mathbf{P}^\beta \mathbf{H} \mathbf{P}^\alpha = \mathbf{H} \mathbf{P}^\beta \mathbf{P}^\alpha = \delta_{\alpha\beta} \mathbf{H} \mathbf{P}^\alpha = \delta_{\alpha\beta} \mathbf{P}^\alpha \mathbf{H} \mathbf{P}^\alpha$  and  $[\mathbf{H}, \mathbf{P}^\alpha] = \mathbf{0}$  and the idempotence of the projectors. Taking into account the previous equations, we get

$$y_i^\beta = \sum_\alpha \sum_j (\mathbf{A}^\beta \mathbf{H} (\mathbf{A}^\alpha)^\text{T})_{ij} x_j^\alpha = \sum_j (\mathbf{A}^\beta \mathbf{H} (\mathbf{A}^\beta)^\text{T})_{ij} x_j^\beta, \quad (\text{B4})$$

which proves the correctness of the matrix-vector multiplication algorithm of Eq. (16).

### APPENDIX C: 1D MINIMUM ENERGY PATH POTENTIAL FOR THE $\theta_i$ COORDINATES

Figure 4 shows the one-dimensional minimum-energy potential along a selected  $\theta_i$  coordinate used to generate potential-optimized DVR points for  $\theta_i$ . This potential was generated by systematically changing  $\theta_i$  and optimizing the remaining 6 angular coordinates (while keeping the distance coordinates fixed at  $r_i = 2.11596 a_0$ ). Next, the one-dimensional Schrödinger equation is solved for this potential using a coordinate-dependent effective mass along the

TABLE III. Correlation table between the irreducible representations of the  $S_5$  and  $S_4$  symmetry groups.

$\Gamma(S_5)$	$\Gamma(S_5) \downarrow S_4$
$A_1$	$A_1$
$A_2$	$A_2$
$G_1$	$A_1 + F_2$
$G_2$	$A_2 + F_1$
$H_1$	$E + F_2$
$H_2$	$E + F_1$
$I$	$F_1 + F_2$

TABLE IV. Character table of the  $S_4$  symmetry group with the induced representation  $\Gamma(S_4) \uparrow S_5$ .

	$E$	$8(234)$	$3(23)(45)$	$6(2345)$	$6(23)$	$\Gamma(S_4) \uparrow S_5$
$A_1$	1	1	1	1	1	$A_1 + G_1$
$A_2$	1	1	1	-1	-1	$A_2 + G_2$
$E$	2	-1	2	0	0	$H_1 + H_2$
$F_1$	3	0	-1	1	-1	$G_2 + H_2 + I$
$F_2$	3	0	-1	-1	1	$G_1 + H_1 + I$

minimum-energy path to generate potential-optimized DVR grid points and basis functions. The coordinate-dependent effective mass has been defined as the inverse of the  $G_{\theta_i, \theta_i}$  matrix element along the minimum energy path.

### APPENDIX D: SUMMARY OF GROUP THEORETICAL DATA AND CONSIDERATIONS FOR $\text{CH}_5^+$

The full symmetry group of  $\text{CH}_5^+$  is  $S_5^* = S_5 \otimes S^*$ , where  $S_5$  is the symmetric group of degree 5,  $S^* = \{E, E^*\}$ , and  $E$  and  $E^*$  denote the identity and inversion operators. Employing the notations introduced in Appendix A, we get  $G = S_5^*$  and  $H = \{E, (45)^*\}$ . This choice for  $H$  can be justified by recognizing that the equilibrium structure of  $\text{CH}_5^+$  has a plane of symmetry ( $C_s$  point group, isomorphic with  $H = \{E, (45)^*\}$ ); according to this specific choice protons 4 and 5 are swapped by reflection through the plane of symmetry in the equilibrium configuration). These considerations imply that  $\text{CH}_5^+$  has  $|G|/|H| = 240/2 = 120$  distinct equilibrium

TABLE V.  $D_{11}^\alpha(g_i)$  irreducible matrix elements (see Eq. (8)) for symmetry operations  $g_i$  of the  $S_4$  symmetry group.

$g_i$	$D_{11}^{A_1}(g_i)$	$D_{11}^{A_2}(g_i)$	$D_{11}^E(g_i)$	$D_{11}^{F_1}(g_i)$	$D_{11}^{F_2}(g_i)$
$E$	1	1	1	1	1
(234)	1	1	-1/2	-1/3	-1/3
(243)	1	1	-1/2	-1/3	-1/3
(345)	1	1	-1/2	-1/3	1
(354)	1	1	-1/2	-1/3	1
(425)	1	1	-1/2	1	-1/3
(452)	1	1	-1/2	1	-1/3
(523)	1	1	-1/2	-1/3	-1/3
(532)	1	1	-1/2	-1/3	-1/3
(23)(45)	1	1	1	-1/3	-1/3
(24)(35)	1	1	1	-1/3	-1/3
(25)(34)	1	1	1	-1/3	-1/3
(2345)	1	-1	-1/2	1/3	-1/3
(2354)	1	-1	-1/2	1/3	-1/3
(2435)	1	-1	1	1/3	-1/3
(2453)	1	-1	-1/2	1/3	-1/3
(2534)	1	-1	1	1/3	-1/3
(2543)	1	-1	-1/2	1/3	-1/3
(23)	1	-1	1	1/3	-1/3
(24)	1	-1	-1/2	-1	-1/3
(25)	1	-1	-1/2	-1	-1/3
(34)	1	-1	-1/2	1/3	1
(35)	1	-1	-1/2	1/3	1
(45)	1	-1	1	-1	1

TABLE VI. Raw list of all  $J = 0$  7D bend terms (in  $\text{cm}^{-1}$ , referenced to the 7D bend zero point wavenumber of  $4016.37 \text{ cm}^{-1}$ ) with  $S_4^*$  symmetry labels, obtained directly from the symmetry-adapted GENIUSH computations.

$A_1^+$	$A_2^+$	$E^+$	$F_1^+$	$F_2^+$	$A_1^-$	$A_2^-$	$E^-$	$F_1^-$	$F_2^-$
0.00	370.87	20.48	59.40	20.19	383.57	9.62	40.82	9.96	58.38
49.21	469.53	58.79	111.55	49.38	567.33	112.23	113.32	41.30	113.44
154.16	635.55	121.24	268.75	111.29	819.34	197.76	139.19	58.00	264.49
329.09	977.45	268.92	359.99	121.45	1150.64	479.33	384.33	112.29	354.72
560.90	1292.85	413.82	369.86	154.26	1367.23	605.44	452.61	138.99	383.18
657.82	1367.54	483.46	468.23	329.04	1437.85	802.01	609.19	264.49	432.16
882.94	1437.83	510.30	509.80	360.25	1480.04	1045.65	640.87	355.02	452.09
1036.80	1471.69	710.67	541.07	411.49	1491.25	1098.83	824.20	384.33	566.79
1069.86	1498.48	716.65	715.93	483.58	1535.73	1114.86	883.61	430.19	609.75
1111.35	1544.22	912.44	729.28	540.21	1575.92	1169.34	970.50	479.64	625.07

configurations and there are 120  $g_a H$  cosets, each of them is associated with one of the distinct equilibrium configurations and has 2 elements. Considering nuclear spin statistics reveals that eigenstates of  $A_1^\pm$ ,  $G_1^\pm$ ,  $H_1^\pm$ , and  $I^\pm$  symmetries violate the Pauli principle (applied to five identical fermions in this case), while the numbers of  $A_2^\pm$ ,  $G_2^\pm$ , and  $H_2^\pm$  eigenstates are 1:4:5.

Let us define a hypothetical ground state wave function  $\phi_+$  localized in the reference potential well and suppose that  $\phi_+$  spans the totally symmetric irreducible representation of  $H$ . If we consider the representation of  $S_5^*$  spanned by 120 symmetry-equivalent ground states  $g_a \phi_+$  localized in different PES wells, we get a reducible representation with the following nonzero characters:  $\chi(E) = 120$  and  $\chi((ij)^*) = 12$  [for all possible  $(ij)^*$  symmetry operations]. Reduction of the representation yields  $A_1^+ \oplus A_2^- \oplus 3G_1^+ \oplus G_1^- \oplus G_2^+ \oplus 3G_2^- \oplus 3H_1^+ \oplus 2H_1^- \oplus 2H_2^+ \oplus 3H_2^- \oplus 3I^+ \oplus 3I^-$ , suggesting that the first 120 computed vibrational eigenstates can be assigned to the ground-state energy level cluster and transform according to the irreducible representations listed above (provided that the tunneling matrix model is applicable to  $\text{CH}_5^+$ ). Repeating the same procedure for an anti-symmetric localized state  $\phi_-$  [so that  $(45)^* \phi_- = -\phi_-$ ] results in another 120-dimensional reducible representation with nonzero characters  $\chi(E) = 120$  and  $\chi((ij)^*) = -12$ , and the following irreducible representation decomposition:  $A_1^- \oplus A_2^+ \oplus G_1^+ \oplus 3G_1^- \oplus 3G_2^+ \oplus G_2^- \oplus 2H_1^+ \oplus 3H_1^- \oplus 3H_2^+ \oplus 2H_2^- \oplus 3I^+ \oplus 3I^-$ . Note that these symmetry arguments say nothing about the energy order of the eigenstates corresponding to different irreducible representations.

As already explained in the main text, due to technical limitations, our treatment is restricted to permutations of the H atoms 2, 3, 4, and 5. This implies that only the  $S_4^* = S_4 \otimes S^*$  symmetry group can be applied, whose elements are enumerated as follows (square brackets indicate conjugacy classes):  $S_4 = \{[E], [(234), (243), (345), (354), (425), (452), (523), (532)], [(23)(45), (24)(35), (25)(34)], [(2345), (2354), (2435), (2453), (2534), (2543)], [(23), (24), (25), (34), (35), (45)]\}$ . Correlation rules between irreducible representations of  $S_5$  and  $S_4$  are presented in Table III.

The construction of group-theoretical projectors requires the character table and the diagonal elements of the symmetry

operation matrices for each irreducible representation [ $D_{ji}^\alpha(g_i)$  in Eq. (8)]. These data for the  $S_4$  symmetry group are summarized in Tables IV and V; they were generated by the GAP program package.<sup>113</sup> Based on these data, the character table and the irreducible matrix elements can be obtained for  $S_4^*$  in a straightforward manner.

## APPENDIX E: LIST OF ALL $J = 0$ 7D BEND ENERGY LEVELS

Table VI contains all  $J = 0$  7D bend energy levels obtained directly from the symmetry-adapted GENIUSH computations. As only the  $S_4^*$  symmetry group can be employed by GENIUSH instead of the full  $S_5^*$  symmetry group, we get each degenerate energy level from two different irreducible representations of the  $S_4^*$  group. Irreducible representations of  $S_5^*$  can be unambiguously assigned to the energy levels by taking into account the correlation rules given in Table III. Moreover, splittings between the in-principle degenerate levels can be used to assess the “internal errors” of the computed energy levels.

<sup>1</sup>M. Quack, *Handbook of High-Resolution Spectroscopy* (Wiley, New York, 2011), Vol. 1, pp. 659–722.

<sup>2</sup>*Symmetrie und Asymmetrie in Wissenschaft und Kunst*, Nova Acta Leopoldina NF Vol. 412, edited by M. Quack and J. Hacker (Wissenschaftliche Verlagsgesellschaft, Stuttgart, 2016), pp. 7–275, with 14 articles from various authors.

<sup>3</sup>C. Lanczos, *J. Res. Natl. Bur. Stand.* **45**, 255 (1950).

<sup>4</sup>H. C. Longuet-Higgins, *Mol. Phys.* **6**, 445 (1963).

<sup>5</sup>M. Quack, *Mol. Phys.* **34**, 477 (1977).

<sup>6</sup>P. R. Bunker and P. Jensen, *Molecular Symmetry and Spectroscopy*, 2nd ed. (NRC Research Press, Ottawa, 1998).

<sup>7</sup>I. M. Mills and M. Quack, *Mol. Phys.* **100**, 9 (2002).

<sup>8</sup>M. Schnell, *Handbook of High-Resolution Spectroscopy* (Wiley, New York, 2011), Vol. 1, pp. 607–632.

<sup>9</sup>T. Oka, *Handbook of High-Resolution Spectroscopy* (Wiley, New York, 2011), Vol. 1, pp. 633–658.

<sup>10</sup>R. M. Whitnell and J. C. Light, *J. Chem. Phys.* **89**, 3674 (1988).

<sup>11</sup>H. Wei and T. Carrington, *J. Chem. Phys.* **101**, 1343 (1994).

<sup>12</sup>A. McNichols and T. Carrington, *Chem. Phys. Lett.* **202**, 464 (1993).

<sup>13</sup>H.-S. Lee, H. Chen, and J. C. Light, *J. Chem. Phys.* **119**, 4187 (2003).

<sup>14</sup>H.-G. Yu, *J. Chem. Phys.* **117**, 2030 (2002).

<sup>15</sup>D. O. Harris, G. G. Engerholm, and W. D. Gwinn, *J. Chem. Phys.* **43**, 1515 (1965).

<sup>16</sup>J. C. Light and T. Carrington, *Adv. Chem. Phys.* **114**, 263 (2000).

<sup>17</sup>X.-G. Wang and T. Carrington, *J. Chem. Phys.* **114**, 1473 (2001).

- <sup>18</sup>X.-G. Wang and T. Carrington, *J. Chem. Phys.* **118**, 6946 (2003).
- <sup>19</sup>B. Poirier, *J. Chem. Phys.* **119**, 90 (2003).
- <sup>20</sup>X.-G. Wang and T. Carrington, *J. Chem. Phys.* **119**, 94 (2003).
- <sup>21</sup>X.-G. Wang and T. Carrington, *J. Chem. Phys.* **119**, 101 (2003).
- <sup>22</sup>X.-G. Wang and T. Carrington, *J. Chem. Phys.* **121**, 2937 (2004).
- <sup>23</sup>X.-G. Wang and T. Carrington, *J. Chem. Phys.* **123**, 154303 (2005).
- <sup>24</sup>R. Marquardt and M. Quack, *J. Chem. Phys.* **109**, 10628 (1998).
- <sup>25</sup>B. J. Braams and J. M. Bowman, *Int. Rev. Phys. Chem.* **28**, 577 (2009).
- <sup>26</sup>S. N. Yurchenko, A. Yachmenev, and R. I. Ovsyannikov, *J. Chem. Theory Comput.* **13**, 4368 (2017).
- <sup>27</sup>NITROGEN, Numerical and Iterative Techniques for Rovibronic Energies with General Internal Coordinates, a program by P. B. Changala, <http://www.colorado.edu/nitrogen>.
- <sup>28</sup>V. L. Tal'roze and A. K. Lyubimova, *Dokl. Akad. Nauk SSSR* **86**, 909 (1952).
- <sup>29</sup>G. A. Olah, *My Search for Carbocations and Their Role in Chemistry*, Les Prix Nobel en 1994 (The Nobel Foundation, Stockholm, 1994), pp. 149–176, Nobel Lecture, 8 December 1994.
- <sup>30</sup>G. A. Olah, *J. Am. Chem. Soc.* **94**, 808 (1972).
- <sup>31</sup>*Carbonium Ions*, edited by G. A. Olah and P. v. R. Schleyer (Wiley, New York, 1968–1976), Vols. 1–5.
- <sup>32</sup>G. A. Olah, *Carbocations and Electrophilic Reactions* (VCH-Wiley Publishers, Weinheim, 1974).
- <sup>33</sup>G. A. Olah, G. K. S. Prakash, K. Wade, Á. Molnár, and R. E. Williams, *Hypercarbon Chemistry*, 2nd ed. (Wiley, Hoboken, NJ, 2011).
- <sup>34</sup>G. A. Olah and G. R. H. Schlosberg, *J. Am. Chem. Soc.* **90**, 2726 (1968).
- <sup>35</sup>G. A. Olah, G. Klopman, and R. H. Schlosberg, *J. Am. Chem. Soc.* **91**, 3261 (1969).
- <sup>36</sup>G. Rasul, G. K. S. Prakash, and G. A. Olah, *Chem. Phys. Lett.* **517**, 1 (2011).
- <sup>37</sup>X.-G. Wang and T. Carrington, *J. Chem. Phys.* **129**, 234102 (2008).
- <sup>38</sup>X.-G. Wang and T. Carrington, *J. Chem. Phys.* **144**, 204304 (2016).
- <sup>39</sup>R. Wodraszka and U. Manthe, *J. Phys. Chem. Lett.* **6**, 4229 (2015).
- <sup>40</sup>I. M. Mills and H. W. Thompson, *Proc. R. Soc. London, Ser. A* **226**, 306 (1954).
- <sup>41</sup>P. R. Bunker and H. C. Longuet-Higgins, *Proc. R. Soc. London, Ser. A* **280**, 340 (1964).
- <sup>42</sup>C. Fábri, J. Sarka, and A. G. Császár, *J. Chem. Phys.* **140**, 051101 (2014).
- <sup>43</sup>J. Sarka, C. Fábri, T. Szidarovszky, A. G. Császár, Z. Lin, and A. B. McCoy, *Mol. Phys.* **113**, 1873 (2015).
- <sup>44</sup>J. Sarka and A. G. Császár, *J. Chem. Phys.* **144**, 154309 (2016).
- <sup>45</sup>J. Sarka, A. G. Császár, S. C. Althorpe, D. J. Wales, and E. Mátyus, *Phys. Chem. Chem. Phys.* **18**, 22816 (2016).
- <sup>46</sup>J. Sarka, A. G. Császár, and E. Mátyus, *Phys. Chem. Chem. Phys.* **19**, 15335 (2017).
- <sup>47</sup>T. Oka, in *Proceedings of 17th Colloquium on High Resolution Molecular Spectroscopy, Nijmegen*, 2001 (Infrared Spectroscopy of  $\text{H}_3^+$ , with discussion of  $\text{CH}_5^+$  spectra and a bet with M. Quack), p. 290.
- <sup>48</sup>E. T. White, J. Tang, and T. Oka, *Science* **284**, 135 (1999).
- <sup>49</sup>O. Asvany, P. Kumar, P. B. Redlich, I. Hegemann, S. Schlemmer, and D. Marx, *Science* **309**, 1219 (2005).
- <sup>50</sup>S. D. Ivanov, O. Asvany, A. Witt, E. Hugo, G. Mathias, B. Redlich, D. Marx, and S. Schlemmer, *Nat. Chem.* **2**, 298 (2010).
- <sup>51</sup>O. Asvany, K. M. T. Yamada, S. Brünken, A. Potapov, and S. Schlemmer, *Science* **347**, 1346 (2015).
- <sup>52</sup>S. Brackertz, S. Schlemmer, and O. Asvany, "Searching for new symmetry species of  $\text{CH}_5^+$  – From lines to states without a model," *J. Mol. Spectrosc.* (to be published).
- <sup>53</sup>P. R. Schreiner, S.-J. Kim, H. F. Schaefer III, and P. v. R. Schleyer, *J. Chem. Phys.* **99**, 3716 (1993).
- <sup>54</sup>H. Müller, W. Kutzelnigg, J. Noga, and W. Klopper, *J. Chem. Phys.* **106**, 1863 (1997).
- <sup>55</sup>A. Brown, A. B. McCoy, B. J. Braams, Z. Jin, and J. M. Bowman, *J. Chem. Phys.* **121**, 4105 (2004).
- <sup>56</sup>Z. Jin, B. J. Braams, and J. M. Bowman, *J. Phys. Chem. A* **110**, 1569 (2006).
- <sup>57</sup>P. R. Bunker, *J. Mol. Spectrosc.* **176**, 297 (1996).
- <sup>58</sup>M. Kolbuszewski and P. R. Bunker, *J. Chem. Phys.* **105**, 3649 (1996).
- <sup>59</sup>A. L. L. East and P. R. Bunker, *J. Mol. Spectrosc.* **183**, 157 (1997).
- <sup>60</sup>A. L. L. East, M. Kolbuszewski, and P. R. Bunker, *J. Phys. Chem. A* **101**, 6746 (1997).
- <sup>61</sup>P. R. Bunker, B. Ostojić, and S. Yurchenko, *J. Mol. Struct.* **695–696**, 253 (2004).
- <sup>62</sup>D. Marx and M. Parrinello, *Nature* **375**, 216 (1995).
- <sup>63</sup>X. Huang, A. B. McCoy, J. M. Bowman, L. M. Johnson, C. Savage, F. Dong, and D. J. Nesbitt, *Science* **311**, 60 (2006).
- <sup>64</sup>G. A. Natanson, G. S. Ezra, G. Delgado-Barrio, and R. S. Berry, *J. Chem. Phys.* **81**, 3400 (1984).
- <sup>65</sup>G. A. Natanson, G. S. Ezra, G. Delgado-Barrio, and R. S. Berry, *J. Chem. Phys.* **84**, 2035 (1986).
- <sup>66</sup>D. M. Leitner, G. A. Natanson, R. S. Berry, P. Villareal, and G. Delgado-Barrio, *Comput. Phys. Commun.* **51**, 207 (1988).
- <sup>67</sup>J. E. Hunter III, D. M. Leitner, G. A. Natanson, and R. S. Berry, *Chem. Phys. Lett.* **144**, 145 (1988).
- <sup>68</sup>M. P. Deskevich and D. J. Nesbitt, *J. Chem. Phys.* **123**, 084304 (2005).
- <sup>69</sup>M. P. Deskevich, A. B. McCoy, J. M. Hutson, and D. J. Nesbitt, *J. Chem. Phys.* **128**, 094306 (2008).
- <sup>70</sup>F. Uhl, E. Walewski, H. Forbert, and D. Marx, *J. Chem. Phys.* **141**, 104110 (2014).
- <sup>71</sup>L. M. Johnson and A. B. McCoy, *J. Phys. Chem. A* **110**, 8213 (2006).
- <sup>72</sup>C. E. Hinkle and A. B. McCoy, *J. Phys. Chem. A* **112**, 2058 (2008).
- <sup>73</sup>C. E. Hinkle and A. B. McCoy, *J. Phys. Chem. A* **113**, 4587 (2009).
- <sup>74</sup>C. E. Hinkle and A. B. McCoy, *J. Phys. Chem. Lett.* **1**, 562 (2010).
- <sup>75</sup>C. E. Hinkle and A. B. McCoy, *J. Phys. Chem. A* **116**, 4687 (2012).
- <sup>76</sup>A. S. Petit, J. E. Ford, and A. B. McCoy, *J. Phys. Chem. A* **118**, 7206 (2014).
- <sup>77</sup>H. Schmiedt, S. Schlemmer, and P. Jensen, *J. Chem. Phys.* **143**, 154302 (2015).
- <sup>78</sup>H. Schmiedt, P. Jensen, and S. Schlemmer, *Phys. Rev. Lett.* **117**, 223002 (2016).
- <sup>79</sup>H. Schmiedt, P. Jensen, and S. Schlemmer, *Chem. Phys. Lett.* **672**, 34 (2017).
- <sup>80</sup>A. G. Császár, C. Fábri, T. Szidarovszky, E. Mátyus, T. Furtenbacher, and G. Czakó, *Phys. Chem. Chem. Phys.* **14**, 1085 (2012).
- <sup>81</sup>E. Mátyus, G. Czakó, and A. G. Császár, *J. Chem. Phys.* **130**, 134112 (2009).
- <sup>82</sup>C. Fábri, E. Mátyus, and A. G. Császár, *J. Chem. Phys.* **134**, 074105 (2011).
- <sup>83</sup>C. Fábri, E. Mátyus, T. Furtenbacher, L. Nemes, B. Mihályi, T. Zoltáni, and A. G. Császár, *J. Chem. Phys.* **135**, 094307 (2011).
- <sup>84</sup>S. N. Yurchenko, R. J. Barber, A. Yachmenev, W. Thiel, P. Jensen, and J. Tennyson, *J. Phys. Chem. A* **113**, 11845 (2009).
- <sup>85</sup>X.-G. Wang and T. Carrington, *J. Chem. Phys.* **138**, 104106 (2013).
- <sup>86</sup>B. T. Sutcliffe and J. Tennyson, *Int. J. Quantum Chem.* **39**, 183 (1991).
- <sup>87</sup>R. Wodraszka and U. Manthe, *J. Phys. Chem. A* **117**, 7246 (2013).
- <sup>88</sup>M. Rey, A. V. Nikitin, and V. G. Tyuterev, *Phys. Chem. Chem. Phys.* **15**, 10049 (2013).
- <sup>89</sup>M. Rey, A. V. Nikitin, and V. G. Tyuterev, *J. Chem. Phys.* **141**, 044316 (2014).
- <sup>90</sup>M. Rey, A. V. Nikitin, and V. G. Tyuterev, *J. Phys. Chem. A* **119**, 4763 (2015).
- <sup>91</sup>E. Mátyus, C. Fábri, T. Szidarovszky, G. Czakó, W. D. Allen, and A. G. Császár, *J. Chem. Phys.* **133**, 034113 (2010).
- <sup>92</sup>C. Eckart, *Phys. Rev.* **47**, 552 (1935).
- <sup>93</sup>T. Szidarovszky, C. Fábri, and A. G. Császár, *J. Chem. Phys.* **136**, 174112 (2012).
- <sup>94</sup>C. Fábri, E. Mátyus, and A. G. Császár, *Spectrochim. Acta, Part A* **119**, 84 (2014).
- <sup>95</sup>S. V. Krasnoshchekov, E. V. Isayeva, and N. F. Stepanov, *J. Chem. Phys.* **140**, 154104 (2014).
- <sup>96</sup>K. Sadri, D. Lauvergnat, F. Gatti, and H.-D. Meyer, *J. Chem. Phys.* **141**, 114101 (2014).
- <sup>97</sup>J. Pesonen, *J. Chem. Phys.* **140**, 074101 (2014).
- <sup>98</sup>V. Szalay, *J. Chem. Phys.* **140**, 234107 (2014).
- <sup>99</sup>V. Szalay, *J. Chem. Phys.* **142**, 174107 (2015).
- <sup>100</sup>V. Szalay, *J. Chem. Phys.* **143**, 064104 (2015).
- <sup>101</sup>A. Yachmenev and S. Yurchenko, *J. Chem. Phys.* **143**, 014105 (2015).
- <sup>102</sup>E. P. Wigner, *Group Theory and its Application to the Quantum Mechanics of Atomic Spectra* (Academic Press, New York, 1959).
- <sup>103</sup>C. Leforestier, L. B. Braly, K. Liu, M. J. Elrod, and R. J. Saykally, *J. Chem. Phys.* **106**, 8527 (1997).
- <sup>104</sup>F. T. Smith, *Phys. Rev. Lett.* **45**, 1157 (1980).
- <sup>105</sup>J. Echave and D. C. Clary, *Chem. Phys. Lett.* **190**, 225 (1992).
- <sup>106</sup>H. Wei and T. Carrington, *J. Chem. Phys.* **97**, 3029 (1992).

- <sup>107</sup>V. Szalay, G. Czakó, Á. Nagy, T. Furtenbacher, and A. G. Császár, *J. Chem. Phys.* **119**, 10512 (2003).
- <sup>108</sup>R. Meyer, *J. Chem. Phys.* **52**, 2053 (1970).
- <sup>109</sup>J. Dai and J. C. Light, *J. Chem. Phys.* **107**, 8432 (1997).
- <sup>110</sup>E. R. Cohen, T. Cvitas, J. G. Frey, B. Holmström, K. Kuchitsu, R. Marquardt, I. Mills, F. Pavese, M. Quack, J. Stohner, H. L. Strauss, M. Takami, and A. Thor, *Quantities, Units and Symbols in Physical Chemistry*, 3rd ed. (Royal Society of Chemistry, 2007).
- <sup>111</sup>B. J. Dalton, *Mol. Phys.* **11**, 265 (1966).
- <sup>112</sup>B. J. Dalton, *J. Chem. Phys.* **54**, 4745 (1971).
- <sup>113</sup>The GAP Group, GAP—Groups, Algorithms, and Programming, version 4.8.7, 2017, <http://www.gap-system.org>.